

304 不锈钢/镍激光焊接中氧对接头形貌、组织及力学性能的影响

董斌鑫^{1,3}, 张艳梅^{1,3}, 虞钢^{1,2,3}, 李少霞^{1,3}, 何秀丽^{1,3*}, 李志永^{1,3**}, 刘宝华⁴

¹中国科学院力学研究所, 北京 100190;

²中国科学院大学材料与光电研究中心, 北京 100049;

³中国科学院大学工程科学学院, 北京 100049;

⁴北京京东方真空电器有限责任公司, 北京 101500

摘要 为了考察保护气氛中氧含量对焊接质量的影响,对 304 不锈钢板和镍板进行了激光焊接实验,研究了不同氧含量下的焊缝形貌、组织、成分、硬度分布以及拉伸性能。结果表明,随着保护气中氧气含量的增加,熔池熔深增大,宽度减小,几何不对称度增大,焊缝表面氧化程度加重。当保护气分别为纯氩气和 21% (体积分数) 氧气时,熔池底部均为柱状晶;当保护气为纯氩气时,熔池顶部为柱状晶和等轴晶的混合晶,加入 21% 氧气后,熔池顶部为等轴晶。加入 21% 氧气后,拉伸强度略有增加,焊缝元素的分布更均匀,晶粒度更小,因此显微硬度增大,且在熔池区域内的变化趋于平缓。活性元素氧改变了表面张力系数,引起了熔池内流动与传热模式的变化,并进一步引起接头形貌、组织与性能的变化。因此,可以通过调整保护气中的氧含量来调控焊接质量。

关键词 激光技术; 异种金属; 激光焊接; 活性元素; 熔池形貌; 显微组织

中图分类号 TG456.7

文献标志码 A

DOI: 10.3788/CJL202249.1602004

1 引言

异种金属焊接不仅能充分利用各组成材料的优异性能,还可以实现轻量化设计,降低整体生产成本,显著提高经济效益,实现资源的最大化利用^[1-5]。因此,在航空航天、汽车制造、电子电器、电池能源及热交换等领域中得到广泛应用。但不同材料在热物性参数、化学成分、冶金性能和力学性能等方面存在差异,这使得异种金属焊接容易出现非均匀混合、脆性金属间化合物与热裂纹等缺陷,焊接熔凝过程更加复杂,焊接质量面临一定的挑战^[6-9]。激光焊接以能量密度集中、热影响区小及可控性好等特点,成为异种金属焊接中重要的先进制造技术之一。

通常情况下,激光焊接需在氩气、氮气等惰性气体中进行,理想情况下熔池不会接触氧气。但由于实际工况的限制以及保护气装置的不足,微量氧气将不可避免地空气进入高温熔池中。此外,一些场景下会利用氧来改变熔池表面张力,比如向焊缝里添加 SiO₂、Ti₂O₃ 等氧化物颗粒^[10-11],或在保护气中掺入一定比例的氧气^[12-13],从而改变焊缝尺寸及性能,因此氧元素对激光焊接具有重要的影响。Sathiya 等^[13]发

现,在惰性气体中焊接超级奥氏体不锈钢时,焊缝形状浅而宽;当加入少量氧气时,焊缝形状从浅宽型变为深窄型,并且产生了更多的初生枝晶体,显微硬度值增大。Hu 等^[14]通过对激光焊接 42CrMo 的实验和数值模拟研究,分析了空气中表面活性元素氧对熔池内流动及传热现象的影响,发现少量的氧可以显著改变熔池的尺寸。Zhao 等^[15]研究了激光点焊过程中不同浓度氧环境下的液态金属流动,发现氧浓度会影响熔池的流动方向以及激光吸收系数,随着氧浓度的升高,熔池的形成时间减少,尺寸增大。上述研究都是针对同种金属的激光焊接,活性元素氧会影响熔池的流动与传热,导致熔池形貌以及组织发生变化。但是,氧元素的含量对异种金属激光焊接的影响还未见报道,尤其是当异种金属由性质差异较大的两种金属组成时,氧元素对其激光焊接焊缝形貌、组织与性能的影响还有待进一步研究。

304 不锈钢和镍的组合被广泛应用于航空航天、石油化工等领域^[16],本文选用 304 不锈钢和镍开展了异种金属的激光焊接实验,研究了保护气中的氧含量对熔池流动以及尺寸的影响,分析了氧元素对焊缝形貌、组织、成分以及性能的影响机制。研究结果为异种

收稿日期: 2021-09-24; 修回日期: 2021-10-27; 录用日期: 2021-11-22

基金项目: 国家自然科学基金(11672304, 11502269)、北京市科技计划项目(Z181100003818015)

通信作者: *xlhe@imech.ac.cn; **lizhiyong@imech.ac.cn

金属激光焊接中活性元素氧的利用、焊缝的保护以及焊接接头的性能调控提供了有益的参考。

2 实验材料及方法

实验材料选用 304 不锈钢(304SS)和纯镍冷轧薄

表 1 304 不锈钢和镍板的化学成分(质量分数,%)

Table 1 Chemical compositions of 304SS and nickel plate (mass fraction,%)

Element	C	P	S	Cr	Ti	Ni	Fe
Ni	0.081	-	0.015	-	0.056	99.700-99.800	0.062
304SS	≤0.080	≤0.045	≤0.030	18.000-20.000	-	8.000-10.500	Bal.

使用德国通快公司的 L1000.1 型 YAG 连续光纤激光器开展实验,最大功率为 1000 W,波长为 1060 nm,激光焊接头被装在五轴数控加工机器人上,设计保护气混合装置,实现氧气和氩气的定量混合,实验装置如图 1 所示。焊接过程中激光束与待焊样件上

板,尺寸为 40 mm×30 mm×1.3 mm,实验前用丙酮清洗样件以去除表面油污。将样件放置在焊接夹具上,保证两个样件上表面平齐。304 不锈钢和镍板的化学成分如表 1 所示。

表面垂直,保护气喷嘴置于激光束后方,与水平面成 50°夹角,距离激光与薄板的作用点 20 mm。焊接实验分别在含有 0、8%、16%、21%(体积分数,全文同)氧气的氧气氩气混合保护气下进行,采用的工艺参数如表 2 所示。

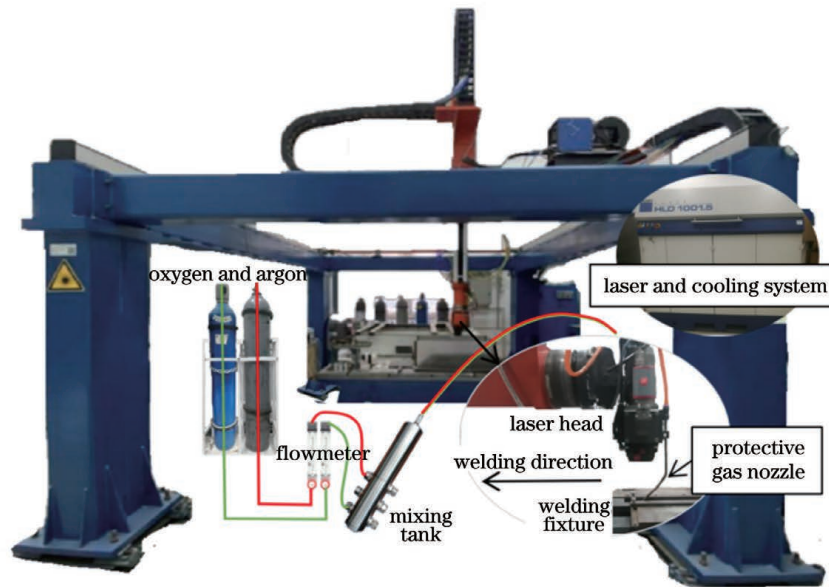


图 1 激光焊接实验装置

Fig. 1 Experimental setup of laser welding

表 2 焊接工艺参数

Table 2 Welding process parameters

Parameter	Laser power /W	Defocusing distance /mm	Radius of laser spot /mm	Welding speed /(mm · s ⁻¹)	Flow of shielding gas /(L · min ⁻¹)
Value	800	-5.5	0.58	20	15

焊后采用线切割机将样件沿垂直焊缝方向切开并镶样,使用标准的金相制样程序研磨和抛光样品,然后在硝酸溶液中进行腐蚀。采用 AM4115ZT 光学显微镜观测焊缝形貌;采用 EM-30AX 台式电镜观测焊缝组织,并测量元素成分;采用 HXD-1000 型数字式显微硬度计测量焊缝硬度;采用 Z250SNS 材料试验机进行室温拉伸强度测试,测试试样为非标试样,采用线切割机切出,尺寸如图 2 所示。

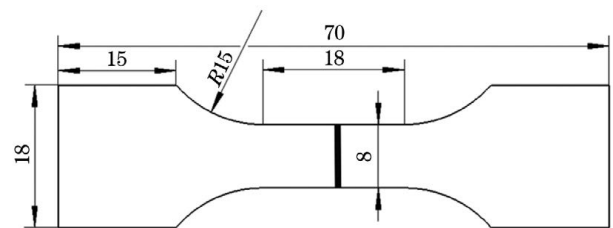


图 2 拉伸试样尺寸示意图

Fig. 2 Dimension diagram of tensile specimen

3 实验结果

3.1 焊缝形貌

观察了 4 种不同氧含量的混合保护气下 304 不锈钢和镍的激光焊接焊缝横截面形貌,如图 3 所示,其中 L' 为熔池宽度, H_{SS} 为 304 不锈钢侧的熔池深度, H_{Ni} 为镍侧的熔池深度。可以看出,焊缝横截面

形貌具有明显的几何非对称特征,其中不锈钢侧的熔化面积与熔化深度较大。氧含量对熔池的形状有着重要的影响。随着氧含量的增加,熔池的深度以及面积明显增大,同时两种金属的熔化面积与熔化深度的差别也随之增大。此外,熔池气液界面处的起伏随保护气中氧含量的增大而明显增多,如图 3 中箭头所示。

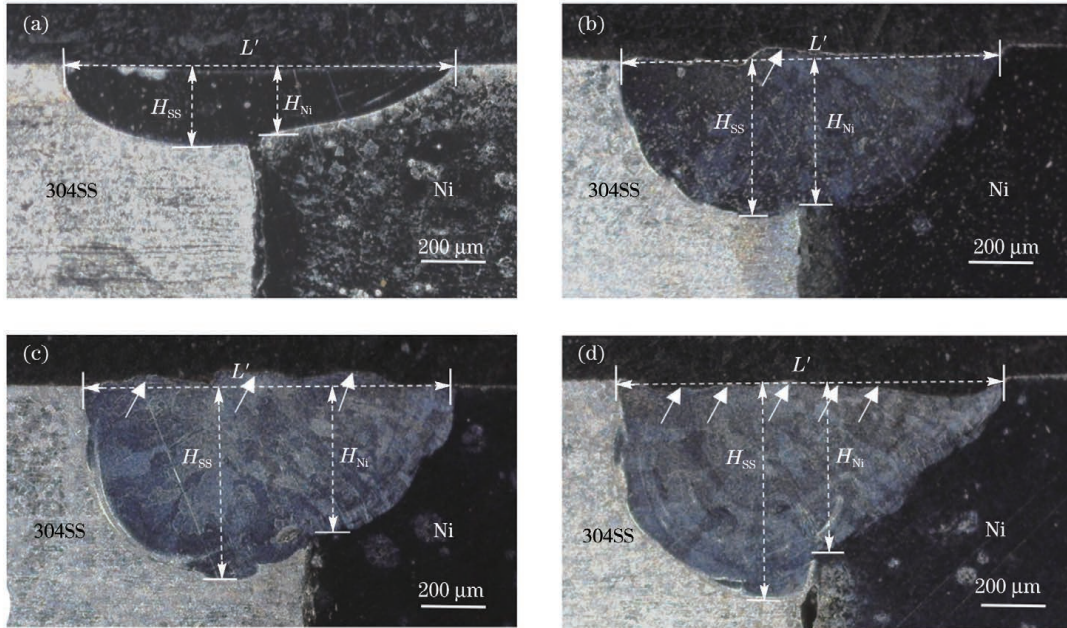


图 3 不同氧气含量下的焊缝横截面形貌。(a) 0%;(b) 8%;(c) 16%;(d) 21%

Fig. 3 Cross-sectional morphologies of weld under different oxygen contents. (a) 0%; (b) 8%; (c) 16%; (d) 21%

不同氧含量下焊缝相应的表面形貌如图 4 所示。焊缝表面在纯氩气保护气氛下为光亮的金属色,且有均匀的鱼鳞纹。随着混合气体中氧气浓度的增加,焊

缝表面发生氧化,颜色加深,鱼鳞纹的破坏程度加重。当混合气中含有 21% 的氧气时,如图 4 (d) 所示,鱼鳞纹几乎全部被破坏。

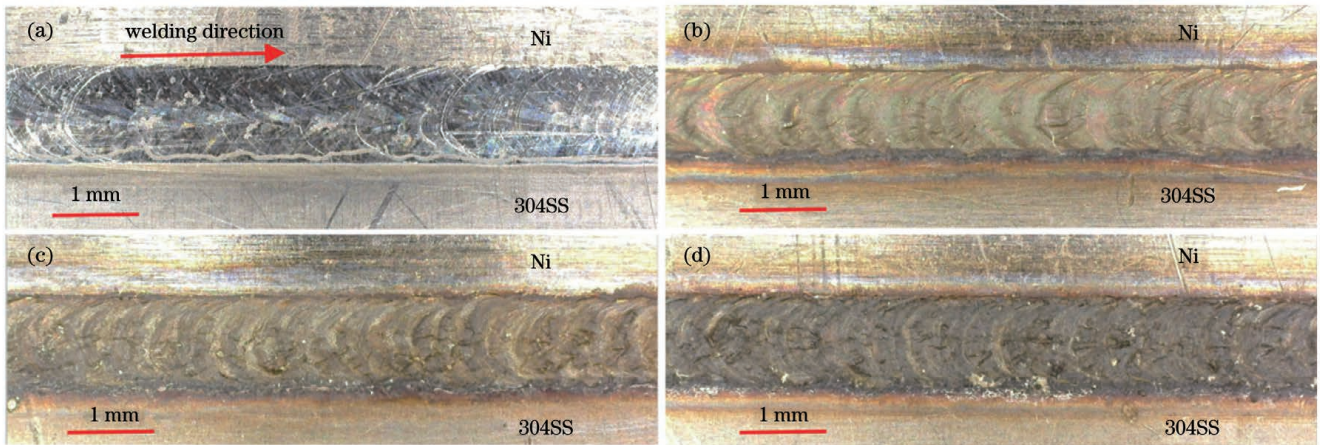


图 4 不同氧气含量下的焊缝表面形貌。(a) 0%;(b) 8%;(c) 16%;(d) 21%

Fig. 4 Surface morphologies of weld seam under different oxygen contents. (a) 0%; (b) 8%; (c) 16%; (d) 21%

对 304 不锈钢和镍的激光焊接熔池宽度、两侧金属的熔池深度以及熔池面积进行测量,结果如图 5 所示。可以看出,随着混合气中氧气含量的增加,焊缝宽度有减小的趋势,深度和面积明显增大,不锈钢侧与镍侧的焊缝深度的差值(图 5 中黑色竖线表示)增大,当混合气中含有 21% 的氧气时,焊缝的最大深度约为纯

氩气时焊缝深度的 2 倍。

3.2 焊缝微观组织

分别对纯氩气和 21% 氧气时 304 不锈钢和镍的激光焊接焊缝的微观组织与成分进行观察与测量,结果分别如图 6 和图 7 所示。选取焊缝处两种金属的典型位置,其微观组织如图 6(c)~(j) 所示。可以看出,

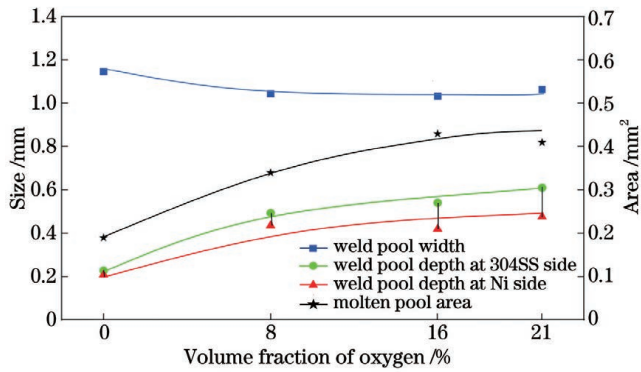


图 5 不同氧气含量下的焊缝尺寸

Fig. 5 Weld sizes under different oxygen contents

在纯氩气的情况下,两侧的底部均为柱状晶;不锈钢侧顶部为等轴晶和柱状晶的混合组织,镍侧顶部的组织

为等轴晶。在 21% 氧气时,两侧的底部也为柱状晶组织;不锈钢侧顶部大部分为等轴晶,并含有较少的树枝晶;镍侧顶部为等轴晶组织。总体上,21% 氧气时焊缝的晶粒尺寸相较于纯氩气时小。

利用能谱仪(EDS)对不同氧气含量下焊缝里的 Fe 元素、Cr 元素、Ni 元素和 O 元素含量进行横向扫描测量,结果如图 7 所示。从图 7(a)可以看出,在纯氩气情况下,从 304 不锈钢侧至镍侧,Fe、Cr 两种元素逐渐减少,而 Ni 元素逐渐增多,熔池中的元素分布不均匀。从图 7(b)可以看出,在 21% 氧气情况下,从 304 不锈钢侧至镍侧,三种元素的含量基本不变,熔池中的元素分布相对比较均匀。两种焊缝中测得的氧元素含量值较小,21% 氧气情况下的焊缝氧含量略高于纯氩气情况下的焊缝氧含量。

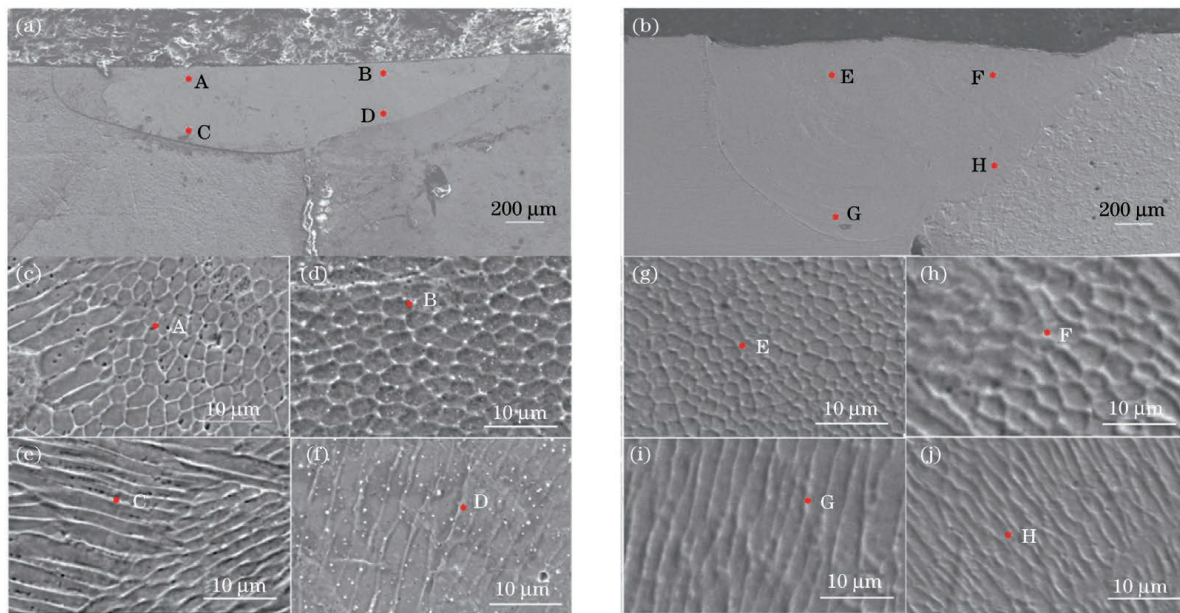


图 6 不同氧气含量下焊缝横截面的微观组织。(a)(b)取点位置;(c)~(j)微观组织

Fig. 6 Cross-sectional microstructures of weld under different oxygen contents. (a) (b) Sampling positions; (c)–(j) microstructures

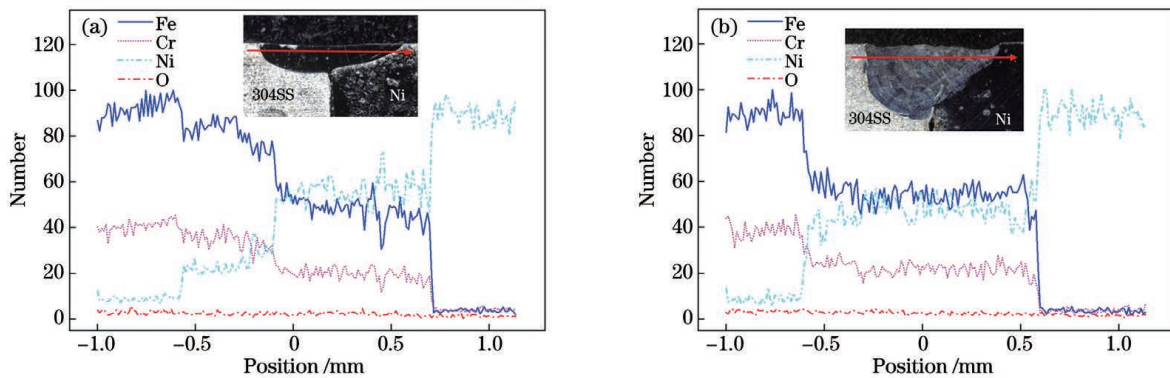


图 7 不同氧气含量下焊缝截面的 EDS 扫描结果。(a) 0%;(b) 21%

Fig. 7 EDS scanning results of weld section under different oxygen contents. (a) 0%; (b) 21%

3.3 焊缝显微硬度及拉伸强度

由上述研究可知,氧元素含量对 304 不锈钢和镍的激光焊接焊缝形貌及凝固组织有重要的影响。为了

进一步分析氧元素含量对力学性能的影响,对 304 不锈钢和镍的激光焊接焊缝进行了显微硬度和拉伸强度测试。在与熔池上表面等间距的位置,沿着熔池宽度

方向测试其显微硬度,结果如图 8 所示。可以看出,21%氧气时,焊缝的显微硬度整体高于纯氩气时的焊缝显微硬度,且熔池内显微硬度值比纯氩气时的更加均匀。对两种条件下的样件进行拉伸测试,均在焊缝热影响区偏镍侧的位置处断开。图 9 为 21%氧气和 0%氧气实验条件下焊接接头的应力-应变曲线,可以看出,21%氧气下的焊接接头拉伸强度(368 MPa)略高于纯氩气条件下的焊接接头拉伸强度(357 MPa)。

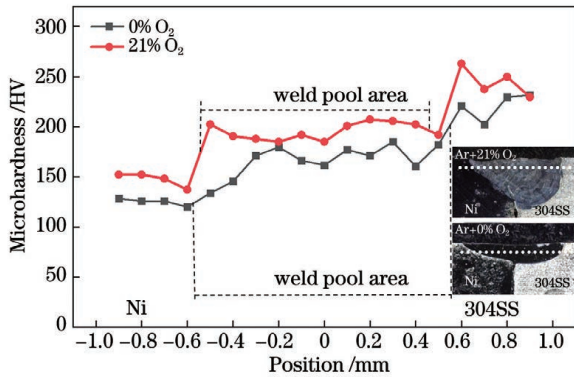


图 8 不同氧气含量下的焊缝显微硬度

Fig. 8 Microhardness of weld under different oxygen contents

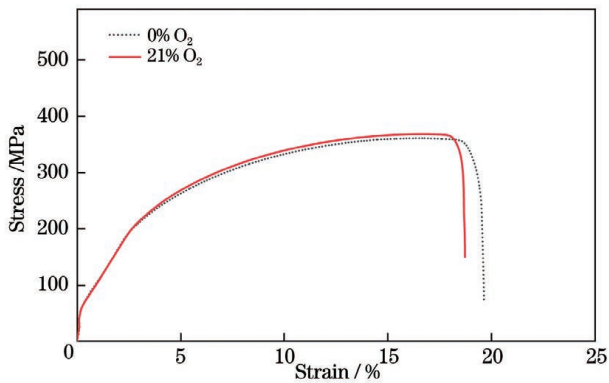


图 9 不同氧气含量下焊接样件的应力-应变曲线

Fig. 9 Stress-strain curves of welding specimen under different oxygen contents

4 分析与讨论

上述实验结果表明,在 304 不锈钢和镍的激光焊

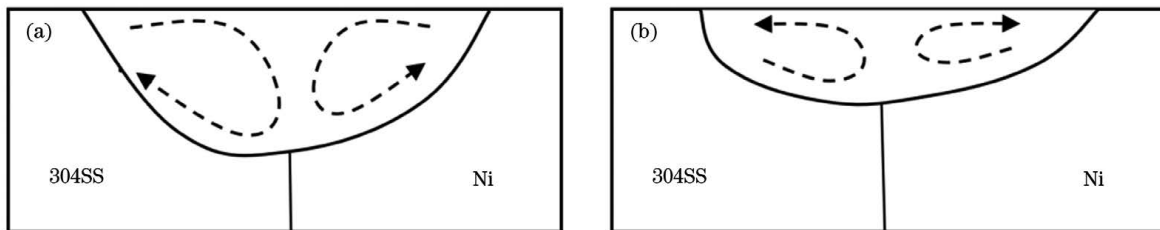


图 10 不同氧气含量下的马兰戈尼对流示意图。(a) 21%;(b) 0%

Fig. 10 Schematics of Marangoni convection under different oxygen contents. (a) 21%; (b) 0%

温度梯度 G 和凝固速率 R 是焊缝凝固过程中重要的凝固参数,它们的乘积 GR 代表冷却速率,决定着最终的晶粒大小, G/R 表征了最终的组织形态^[23]。活性元素氧的存在影响了熔池的流动方向,改变了熔

接过程中,焊缝受保护气中氧的含量的影响。在不同氧含量情况下,焊缝的宏观形貌、微观组织以及性能不同。氧是常见的活性元素,实验研究^[16-19]和数值模拟^[1,18]的结果表明,表面活性元素会影响材料的表面张力系数。当金属表面活性元素的含量增大到一定程度时,表面张力系数出现由负到正的符号转变,从而使熔池的流动模式发生变化^[14]。对比实验中不同氧气含量情况下的熔池尺寸,在氩气中混入氧气后,氧的存在使得表面张力系数由负值变为正值,熔池中心处的表面张力大于熔池外侧,熔池内的液态金属流动方向会发生改变,熔池上层的液态金属从外侧流向熔池中心,如图 10(a)所示,液态金属吸收的激光能量被输运至熔池底部,熔池宽度减小,深度增加。在纯氩气的情况下,认为没有表面活性元素氧,金属表面张力系数为负,熔池外侧的表面张力大于中心处,液态金属由熔池中心流向外侧,因此熔池流体由内向外运动,如图 10(b)所示。该种自内向外的流体流动导致熔池宽度增加,熔深较小。

同时,对流和扩散是合金元素输运的两种主要机制^[20]。由于元素浓度差的存在,合金元素由两侧基体向熔池中间扩散。在 21%氧气情况下,对流方向为从外侧流向熔池中心,这与元素扩散的方向趋于一致,促进了不同元素向中心的扩散,元素混合趋向均匀。对于纯氩气的情况,对流方向为从熔池中心流向外侧,与金属元素的扩散方向相反,减弱了合金元素的混合效果。所以,对比 21%氧气的情况,纯氩气时熔池中心的元素分布不均匀。

304 不锈钢和镍的热物性参数的差异^[21-22]引起了熔池不对称现象,其中不锈钢的热导率较低。同时不锈钢的熔点低于纯镍(304 不锈钢的熔点为 1672 K,镍的熔点为 1730 K),在同样的热输入下,热累积比镍更多,不锈钢熔化得更多,所以焊缝不锈钢侧的熔池深且面积较大。焊缝表面由于氧气的存在,发生氧化。而且随着氧气浓度的增大,氧化程度加强,颜色加深,表层金属与氧气发生作用,产生了不稳定的氧化物,发生表面剥落现象,破坏了鱼鳞纹。

池的形状,而熔池的形状对凝固过程中的温度梯度和凝固速率有着重要影响。图 11 所示为 21%氧气和纯氩气时不锈钢和镍激光焊接过程中的熔池凝固前沿示意图。凝固速率 $R = V \times \cos \alpha$,其中 V 为焊接速度, α

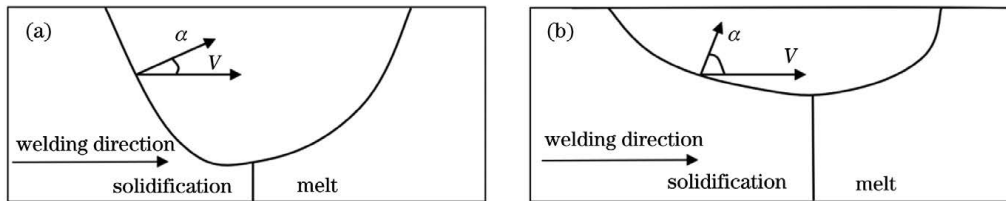


图 11 不同氧气含量下的熔池凝固前沿示意图。(a) 21%;(b) 0%

Fig. 11 Schematics of solidification front of molten pool under different oxygen contents. (a) 21%; (b) 0%

为固液界面法线与焊接方向的夹角^[24]。活性元素氧改变了熔池形貌与对流方向,由图 3 的熔池截面可以推测,21% 氧气时的熔池凝固前沿几乎呈竖直,如图 11(a)所示;纯氩气时凝固前沿较平缓,如图 11(b)所示。从熔池底部到顶部,21% 氧气时的 R 迅速增大,纯氩气时的 R 缓慢增大。当熔池底部的 G/R 值较大时,21% 氧气和纯氩气条件下均存在柱状晶。从熔池底部到顶部,纯氩气时的 G/R 减小较慢,顶部为柱状晶和等轴晶的混合晶;21% 氧气时 G/R 减小较快,顶部为等轴晶。同时,21% 氧气时冷却速率 GR 也较大,因此晶粒更细小,显微硬度以及拉伸强度较高。氧的存在可能会导致产生金属氧化物,进一步提高了焊缝的显微硬度,21% 氧气时三种主要元素的分布均匀,晶粒尺寸相近,故熔池区域的显微硬度测量值较为一致。

对于异种金属的激光焊接,保护气体中活性元素氧的含量影响了熔池中流体流动的方式,从而影响了焊接接头的形貌、组织和性能。活性元素氧提高了不锈钢和镍的焊接接头的显微硬度和拉伸性能,但同时氧的存在使其表面发生氧化,表面颜色加重且变得粗糙,此外,研究表明,氧还会造成焊接气孔及母材氧化失效等问题^[23]。因此,在异种金属的激光焊接过程中,可以根据不同的材料体系以及服役需求,通过控制保护气中氧气的含量来调控焊接质量,最终获得所需的焊接接头。

5 结 论

在不同氧气含量的混合保护气氛下,对 304 不锈钢板和镍板进行了激光焊接实验,分析了氧含量对焊缝形貌、组织与性能的影响,得到以下结论。

1) 活性氧元素的存在改变了马兰戈尼对流的方向,熔池由自内向外的流动转变为自外向内的流动,熔池形状由浅宽变为深窄,熔池面积增大。

2) 在 21% 氧气时,焊缝元素的分布更加均匀,熔池顶部主要为等轴晶,底部为柱状晶;在纯氩气的情况下,顶部为等轴晶和柱状晶的混合晶,底部为柱状晶。21% 氧气时的晶粒尺寸小于纯氩气时的晶粒尺寸。

3) 由于焊缝的晶粒尺寸小且主要合金元素分布均匀,21% 氧气时的显微硬度高于纯氩气时的显微硬度。随着氧含量的增加,焊缝表面质量变差。因此可以通过调整保护气中的氧含量来调控焊接的质量。

4) 随着保护气中氧含量的增加,熔池内液态金属对流的驱动力与流动模式发生转变,焊缝熔池深度、面积以及两侧金属熔池的不对称度均有增大的趋势,金属元素混合均匀,但晶体尺寸减小,显微硬度以及拉伸强度均增大。

氧元素影响下熔池的动态演化、流动模式转变的临界温度及氧浓度等还有待研究,下一步工作将结合数值模拟手段,进一步深入研究氧含量对焊接接头的影响。

参 考 文 献

- [1] Reising U, Schleser M, Mokrov O, et al. Optimization of laser welding of DP/TRIP steel sheets using statistical approach[J]. Optics & Laser Technology, 2012, 44(1): 255-262.
- [2] Esfahani M N, Coupland J, Marimuthu S. Microstructure and mechanical properties of a laser welded low carbon-stainless steel joint[J]. Journal of Materials Processing Technology, 2014, 214(12): 2941-2948.
- [3] Hu Y W, He X L, Yu G, et al. Capillary convection in pulsed-butt welding of miscible dissimilar couple[J]. Proceedings of the Institution of Mechanical Engineers, Part C: Journal of Mechanical Engineering Science, 2017, 231(13): 2429-2440.
- [4] 李继红, 雷龙宇, 杜明科, 等. T2 铜/304 不锈钢激光焊接接头组织及性能研究[J]. 激光与光电子学进展, 2022, 59(13): 1316001.
Li J H, Lei L Y, Du M K, et al. Study on microstructure and properties of T2 copper/304 stainless steel laser welded joint[J]. Laser & Optoelectronics Progress, 2022, 59(13): 1316001.
- [5] 尚大智, 张健, 冯爱新, 等. 焊面结构化对铜/钢激光焊接接头组织及力学性能的影响[J]. 中国激光, 2020, 47(9): 0902004.
Shang D Z, Zhang J, Feng A X, et al. Effect of surface texturization on microstructure and mechanical properties of laser welded copper/steel joint[J]. Chinese Journal of Lasers, 2020, 47(9): 0902004.
- [6] Mukherjee S, Chakraborty S, Galun R, et al. Transport phenomena in conduction mode laser beam welding of Fe-Al dissimilar couple with Ta diffusion barrier[J]. International Journal of Heat and Mass Transfer, 2010, 53(23/24): 5274-5282.
- [7] Torkamany M J, Tahamtan S, Sabbaghzadeh J. Dissimilar welding of carbon steel to 5754 aluminum alloy by Nd:YAG pulsed laser[J]. Materials & Design, 2010, 31(1): 458-465.
- [8] 虞钢, 何秀丽, 李少霞. 激光先进制造技术及其应用[M]. 北京: 国防工业出版社, 2016: 15-28.
- [9] Yu G, He X L, Li S X. Laser manufacturing and its applications[M]. Beijing: National Defense Industry Press, 2016: 15-28.
- [9] 谷晓燕, 朱开轩, 隋成龙, 等. 镁合金/钛合金脉冲激光焊接头的组织、性能调控[J]. 中国激光, 2020, 47(1): 0102005.
Gu X Y, Zhu K X, Sui C L, et al. Control of microstructure and property of pulse laser welded joint of magnesium/titanium alloy[J]. Chinese Journal of Lasers, 2020, 47(1): 0102005.
- [10] Modenesi P J, Apolinário E R, Pereira I M. TIG welding with single-component fluxes[J]. Journal of Materials Processing

- Technology, 2000, 99(1/2/3): 260-265.
- [11] Kaul R, Ganesh P, Singh N, et al. Effect of active flux addition on laser welding of austenitic stainless steel [J]. Science and Technology of Welding and Joining, 2007, 12(2): 127-137.
- [12] 赵琳, 塚本进, 荒金吾郎, 等. 激光-电弧复合焊接保护气体 O₂ 含量对焊缝均匀性和熔池流动的影响 [J]. 中国激光, 2015, 42(6): 0603006.
- Zhao L, Tsukamoto S, Arakane G, et al. Influence of shielding oxygen content on weld homogeneity and fluid flow in laser-arc hybrid welding [J]. Chinese Journal of Lasers, 2015, 42(6): 0603006.
- [13] Sathiyaraj P, Mishra M K, Shanmugarajan B. Effect of shielding gases on microstructure and mechanical properties of super austenitic stainless steel by hybrid welding [J]. Materials & Design, 2012, 33: 203-212.
- [14] Hu Y W, He X L, Yu G, et al. Experimental and numerical study on laser keyhole welding of 42CrMo under air and argon atmosphere [J]. The International Journal of Advanced Manufacturing Technology, 2017, 90(9/10/11/12): 3555-3565.
- [15] Zhao C X, Kwakernaak C, Pan Y, et al. The effect of oxygen on transitional Marangoni flow in laser spot welding [J]. Acta Materialia, 2010, 58(19): 6345-6357.
- [16] Zhao C X, Richardson I M, Kenjeres S, et al. A stereo vision method for tracking particle flow on the weld pool surface [J]. Journal of Applied Physics, 2009, 105(12): 123104.
- [17] Heiple C R, Roper J R, Stagner R T, et al. Surface-active element effects on the shape of GTA, laser, and electron-beam welds [J]. Welding Journal Research Supplement, 1983, 62(3): 72.
- [18] Lu S P, Dong W C, Li D Z, et al. Numerical simulation for welding pool and welding arc with variable active element and welding parameters [J]. Science and Technology of Welding and Joining, 2009, 14(6): 509-516.
- [19] Sahoo P, Debroy T, McNallan M J. Surface tension of binary metal: surface active solute systems under conditions relevant to welding metallurgy [J]. Metallurgical Transactions B, 1988, 19(3): 483-491.
- [20] Gan Z T, Yu G, He X L, et al. Surface-active element transport and its effect on liquid metal flow in laser-assisted additive manufacturing [J]. International Communications in Heat and Mass Transfer, 2017, 86: 206-214.
- [21] Li Z Y, Yu G, He X L, et al. Effects of interface conditions on heat and mass transfer during modeling of laser dissimilar welding [J]. Proceedings of the Institution of Mechanical Engineers, Part C: Journal of Mechanical Engineering Science, 2022, 236(3): 1616-1630.
- [22] Li Z Y, Yu G, He X L, et al. Probing thermocapillary convection and multisolute dilution in laser welding of dissimilar miscible metals [J]. International Journal of Thermal Sciences, 2022, 172: 107242.
- [23] Kou S. Weldingmetallurgy [M]. Hoboken: John Wiley & Sons Inc., 2003: 17-20.
- [24] 陈茹, 虞钢, 何秀丽, 等. 38MnVS6 钢中硫元素扩散对激光熔覆涂层形貌和组织的影响 [J]. 中国激光, 2018, 45(6): 0602005.
- Chen R, Yu G, He X L, et al. Effect of sulfur diffusion in 38MnVS6 steel on morphology and microstructure of laser cladding layers [J]. Chinese Journal of Lasers, 2018, 45(6): 0602005.

Effects of Oxygen on Morphology, Microstructure and Mechanical Property of Joint in Laser Welding of 304 Stainless Steel and Nickel

Dong Binxin^{1,3}, Zhang Yanmei^{1,3}, Yu Gang^{1,2,3}, Li Shaoxia^{1,3}, He Xiuli^{1,3*}, Li Zhiyong^{1,3**},
Liu Baohua⁴

¹Institute of Mechanics, Chinese Academy of Sciences, Beijing 100190, China;

²Center of Materials Science and Optoelectronics Engineering, University of Chinese Academy of Sciences, Beijing 100049, China;

³School of Engineering Science, University of Chinese Academy of Sciences, Beijing 100049, China;

⁴Beijing Orient Vacuum Electric Co., Ltd., Beijing 101500, China

Abstract

Objective Laser welding of dissimilar metals is an important welding method, which is widely used in aerospace, automobile manufacturing, electronics, battery energy, and other industries. In laser welding, the active element oxygen in air is inevitably absorbed by the weld pool, but in some welding technologies, specific quality adjustments can be made by adding oxygen to wires. Some scholars have studied the effects of oxygen on the weld pool flow, weld pool size, and laser welding properties. However, the effects of oxygen on laser welding of dissimilar metals are reported, especially the effects of oxygen on the weld morphology, microstructure, and properties of dissimilar metal with large different thermal-physical parameters, chemical compositions, and mechanical performances. Here, 304 stainless steel (304SS) and nickel are selected for the experiments of laser welding of dissimilar metals. The effects of oxygen content in the shielding gas on weld pool morphology and dimension, solidified microstructure, alloy element dilution, and mechanical properties are analyzed. This research provides useful references for the utilization and protective effect of active element oxygen in laser welding of dissimilar metals and the performance regulation of welded joints.

Methods The experiments are conducted on a five-axis numerical control machining robot, using a continuous fiber laser with a wavelength of 1060 nm. A protective gas mixing device is designed to realize the quantitative mixing of oxygen and argon. The 304SS and pure nickel plates (40 mm × 30 mm × 1.3 mm) are used as the experimental materials. The welding experiments are first conducted under the mixed shielding gas of oxygen and argon, and the volume fraction of

oxygen changes from 0, 8%, 16% to 21% (volume fraction) in the parametric study. Then, the weld pool morphology, solidified microstructure, and alloy element distribution of the obtained metallographic samples are observed by optical microscopy, scanning electron microscopy (SEM), and energy dispersive spectrometer (EDS), respectively. Finally, the material testing machine is used to test the tensile strength.

Results and Discussions The cross-sectional morphology of weld has the obvious geometric asymmetry, in which the melted area and melted depth at the 304SS side are large. With the increase of oxygen content, the weld width decreases, but the weld depth and melted area increase (Fig. 5). Besides, the weld surface is oxidized seriously due to the increased oxygen content (Fig. 4). When oxygen is mixed into the shielding gas, the surface tension coefficient changes from negative to positive, resulting in the change of the flow mode of the weld pool. As a result, the energy absorbed by the liquid metal from the laser is transported to the bottom of the weld pool, which reduces the width and increases the depth of the weld pool. The smaller thermal conductivity and liquidus temperature of 304SS lead to a deeper and larger weld pool as well as a larger melted area at the 304SS side. The value of the morphological parameter G/R [the ratio of temperature gradient (G) to solidification rate (R)] at the bottom of the weld pool is larger, and the columnar dendrites exist in the cases of 21% oxygen and pure argon. From the bottom to the top of the weld pool, the G/R decreases slowly in the case of pure argon, and the top is the mixed dendrites of columnar dendrites and equiaxed dendrites. In the case of 21% oxygen, G/R decreases rapidly, and the top is the equiaxed dendrites (Fig. 6). The cooling rate GR in the case of 21% oxygen is also large, and the microstructure is fine. Due to the smaller scale of microstructure, the microhardness (Fig. 8) and tensile strength (Fig. 9) are high in the case of 21% oxygen. Additionally, the presence of oxygen might produce metal oxides to further improve the microhardness of the weld. Due to the concentration gradient, the alloy elements diffuse from the matrix at both sides to the middle of the weld pool. In the case of 21% oxygen, the convection flows from the fusion boundary to the center of the weld pool, which is consistent with that for the element diffusion, and promotes the dilution of different elements to the center. Thus, the element mixing in the case of 21% oxygen tends to be more uniform. In the case of pure argon, the results are opposite (Fig. 7).

Conclusions In present study, laser welding experiments are conducted on the 304SS and nickel plates under mixed protective atmosphere with different oxygen contents and the effects of oxygen content on weld morphology, microstructure, and properties are analyzed. Because of the active element oxygen, the direction of Marangoni convection changes to be opposite, the shape of weld pool also changes from shallow and wide to deep and narrow, and the area of weld pool extends. In the case of 21% oxygen, the distributions of alloy elements are more uniform. The solidified microstructure is mainly the equiaxed dendrites on the top of weld pool and the columnar dendrites at the bottom. In the case of pure argon, the microstructure in the top area is the mixed crystal of equiaxed dendrites and columnar dendrites, in contrast, and that at the bottom is columnar dendrites. Due to the fine microstructure of the weld, the microhardness in the case of 21% oxygen is higher than that in the case of pure argon. However, with the increase of oxygen content, the weld surface quality becomes worse. Therefore, the welding quality can be controlled to a certain extent by adjusting the oxygen content in the shielding gas. With the increase of oxygen content in the shielding gas, the driving force and flow mode of liquid metal convection in the weld pool change, which increases the depth and melted area of weld pool and makes the asymmetry of weld pool at both sides more obvious. Furthermore, when the oxygen content increases, the metal elements are mixed more uniformly, and the microstructural morphology is almost unchanged. However, the microstructural size decreases, and the microhardness and tensile strength increase.

Key words laser technique; dissimilar metals; laser welding; active element; melt pool morphology; microstructure